Communications in Computational Chemistry
Commun. Comput. Chem., Vol. 7, No.1 , 202–208
doi: 10.4208/cicc.2025.85.02

Regular Article

Insights into the Stability and Photophysical Properties of Expanded Porphyrins Through Theoretical Calculation

Wei Wei[1,*], Zeng-Xia Zhao[1], Xiao-Li Sun[1], Xi Chen[3], Bin Hu[1,*] and Wei Li[2,*]

[1]*College of Chemistry, Jilin University, Changchun 130012, P. R. China;*

[2]*School of Chemistry and Materials Science, Hunan Agricultural University, Changsha, China;*

[3]*College of Chemistry and Chemical Engineering, Northeast Petroleum University, Daqing, 163318, China.*

[*] Corresponding authors: weiweiww@jlu.edu.cn; hubin_80@jlu.edu.cn; weili@hunau.edu.cn

Received on 25 March 2025; Accepted on 26 April 2025

Abstract: Expanded porphyrins serve as promising candidates for MRI contrast agents and sensitizers in photodynamic therapy. In this study, we theoretically designed a series of expanded porphyrins incorporating thiophene and selenophene moieties to investigate their optoelectronic properties. Density functional theory (DFT) and time-dependent DFT (TD-DFT) calculations were performed to assess their aromaticity, stability, and photophysical characteristics. Our results reveal that all designed molecules exhibit superior optoelectronic performance, with enhanced aromaticity compared to conventional porphyrins. The absorption spectra of the molecules closely resemble that of porphyrins, suggesting potential applicability in related biomedical and photonic applications. Notably, molecule 4, featuring both a thiophene moiety and a conventional selenophene ring, demonstrates the highest stability, an increased energy gap highest between occupied molecular orbital (HOMO) and lowest unoccupied molecular orbital (LUMO), and a planar geometry, leading to strengthened aromaticity. These findings provide valuable insights for the rational design of next-generation porphyrin-based materials.

Key words: excited state, aromaticity, stability, optoelectronic properties, expanded porphyrins.

1. Introduction

Porphyrins, renowned for their fundamental roles in biological systems, have attracted significant interest in theoretical chemistry due to their well-defined electronic structures and diverse applications. In particular, 18 π-electron porphyrins have been extensively studied for their potential in material science, pigment development, and medicinal applications [1–5]. Structurally, these molecules consist of four pyrrole subunits connected in a coplanar arrangement via methine carbon bridges at their α-carbon positions.

As higher homologues of conventional porphyrins, expanded porphyrins have emerged as a major research focus over the past four decades [6–10]. These systems, characterized by enlarged cavities and extended conjugation, exhibit unique electronic properties and structural flexibility, making them promising candidates for various applications in theoretical chemistry. Their ability to bind diverse substrates depends on both the specific porphyrin framework and cavity dimensions. In neutral expanded porphyrins, aromatic conjugation primarily involves the imine-type nitrogen atoms, while the amino NH groups remain non-conjugated. Additionally, expanded porphyrins display distinctive Hückel and Möbius topologies compared to conventional tetrapyrrolic porphyrin macrocycles [11], enhancing their utility in biomedical applications such as MRI contrast agents and sensitizers for photodynamic therapy [12]. Several expanded porphyrins have garnered attention in contemporary research. Notably, sapphyrin [13,14], a pentapyrrolic expanded porphyrin with a 22 π-electron aromatic

system, stands out due to its structural modifications. Unlike porphyrin, sapphyrin features an additional pyrrole inserted between a meso-carbon and an α-pyrrolic position. Other derivatives, including carbasapphyrin [15], benzosapphyrin [16], and dithiabenzisapphyrin [17], exhibit distinct aromaticity, stability, and absorption properties, contributing to their growing significance in optoelectronic applications [18].

Thiophene has emerged as a widely used π-conjugated building block, often replacing pyrrole units within the porphyrin framework [19]. Incorporating heterocyclic rings such as furan, thiophene [20,21], or selenophene [22,23] into expanded porphyrins enhances their aromatic stability and optoelectronic properties. These modified porphyrins, whether featuring normal or inverted thiophene/selenophene configurations, display remarkable photophysical characteristics [24]. Given this, it is crucial to explore how these structural modifications influence the aromaticity, stability, and electronic behavior of expanded porphyrins.

In this study, we theoretically design and analyze four macrocyclic molecules (coded as **1–4** in Scheme 1) incorporating thiophene and selenophene subunits. Using high-level quantum chemistry calculations, we systematically investigate their aromaticity, stability, and photophysical properties. Furthermore, we assess the impact of conventional versus inverted thiophene and selenophene configurations on their optoelectronic behavior. By elucidating the relationship between structural modifications and electronic properties, this work aims to advance the rational design of novel porphyrin-based materials with enhanced functionalities, contributing to the development of next-generation materials in theoretical chemistry and material science.

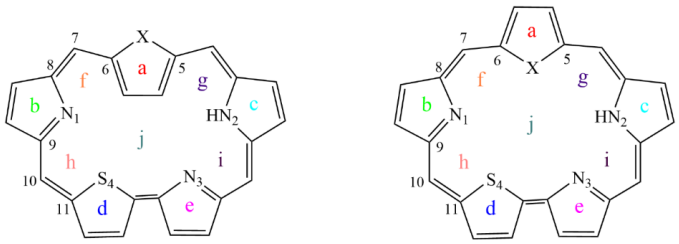

Scheme 1. Sketch structures of molecules of **1-4.**

2. Computational details

All calculations were conducted utilizing density functional theory (DFT) and time-dependent density functional theory (TD-DFT) methods. The full optimization of compounds **1-4** was executed using the DFT-B3LYP6-311G (d, p) level of theory [25-28]. To ensure structural stability, vibrational frequencies were computed for the optimized structures at the same theory level, confirming the absence of imaginary frequencies and validating that the obtained structures represent local energy minima. Vertical electronic excitations were determined via TD-DFT calculations using the range-separated CAM-B3LYP functional combined with a 6-311G (d, p) basis set. Additionally, aromatic stabilization energy (ASE) [29] values were computed employing a ring-opening isobond chemical reaction. Positive reaction energies indicate aromaticity, while negative values suggest antiaromaticity. The ASE was evaluated using the B3LYP functional alongside a 6-311G (d, p) basis set. All calculations were performed using the Gaussian 16 software package [30].

Critical points are analyzed at specific locations relative to the molecular structure. To avoid in-plane components, nucleus-independent chemical shifts (NICS) values are calculated at designated points, such as 1 Å above the thiophene/selenophene ring (point a), at the geometrical center of the pyrrole ring (points b, c, and e), above the thiophene ring (point d), and at various intramolecular positions (points f, g, h, and i), as well as at the molecular center (point j), using the GIAO method. In this study, calculations were performed using several functionals (CAM-B3LYP, M05-2X, M06-2X) to assess their performance. NICS (1) zz values obtained with the CAM-B3LYP functional closely match those from the M05-2X and M06-2X functionals. Therefore, CAM-B3LYP is selected as the optimal functional due to its widespread usage. Molecules are deemed aromatic if the NICS(1)zz value is negative, while a positive value suggests antiaromaticity. Illustrations of the different critical points are depicted in Scheme 1. The critical points were analyzed using the 'atoms in molecules' theory of Bader [31] via the AIM2000 package [32]. An NBO analysis [33] is also performed to calculate the second-order perturbation at the B3LYP/6-311G (d,p) theory level.

3. Results and discussions

3.1 Geometrical structures

The optimized ground-state structures of the designed molecules were obtained using the B3LYP/6-311G(d,p) level of theory, as shown in Figure 1. Notably, molecules **1** and **2** adopt inverted configurations, whereas molecules **3** and **4** feature conventional structures. These molecules were designed by substituting the pyrrole unit in the porphyrin core with either a thiophene or selenophene moiety. Specifically, molecules **3** and **4** incorporate the standard orientations of thiophene and selenophene, respectively. Structural interconversion between these configurations occurs via rotation of the thiophene/selenophene ring, transforming molecule **1** into **3** and molecule **2** into **4**. Table 1 summarizes the key optimized geometric parameters, providing insights into the structural characteristics of the designed molecules.

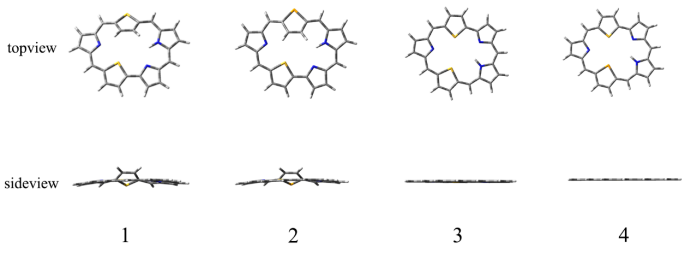

Figure 1. Optimized ground state structures of molecules **1-4.**

The N1-N2 bond lengths for molecules **1**, **2**, **3**, and **4** are 6.021, 6.084, 6.254, and 6.302 Å, respectively. Similarly, the C5-N3 bond lengths measure 4.835, 4.882, 5.271, and 5.312 Å, while the C6-S4 bond lengths are 4.349, 4.401, 4.838, and 4.857 Å. These values show a clear increasing trend in the order of **1** < **2** < **3** < **4**. Regarding bond angles, the C6-C7-C8 angles for molecules **1**–**4** are 121.7º, 122.4º, 127.5º, and 129.4º, respectively, with a similar trend observed for the

Table 1. Main optimized geometry structure parameters of **1**-**4** in the ground state.

	1	**2**	**3**	**4**
Bond lengths (Å)				
N1-N2	6.021	6.084	6.254	6.302
C5-N3	4.835	4.882	5.271	5.312
C6-S4	4.349	4.401	4.838	4.857
Bond angles (°)				
C6-C7-C8	121.7	122.4	127.5	129.4
C9-C10-C11	125.3	125.5	126.4	127.1
Dihedral angles (°)				
C6-C7-C8-N1	10.1	9.7	0.0	0.0
C9-C10-C11-S4	0.6	0.4	0.0	0.0

C9-C10-C11 angles. Dihedral angles of C6-C7-C8-N1 and C9-C10-C11-S4, listed in Table 1, further highlight structural differences. Notably, molecules **3** and **4** exhibit nearly zero dihedral angles, indicating enhanced coplanarity. In contrast, molecules **1** and **2** feature a perpendicular thiophene/selenophene unit relative to the porphyrin core, while the rest of the macrocycle remains nearly coplanar. To assess aromaticity and stability, we employed the aromatic stabilization energy (ASE) method, previously used to evaluate five-membered rings in the ground state. ASE provides an energetic measure of aromaticity, with larger values indicating greater stability. Calculations referenced thiophene, selenophene, pyrrole, and five-membered rings with localized single and double bonds (see Scheme 2) [34]. As shown in Table 2, ASE values follow the trend **4** > **3** > **2** > **1**, indicating a progressive decrease in stability from molecule **4** to molecule **1**.

Table 2. Computed aromatic stabilization energy (ASE, in kcal/mol) of molecules **1**-**4**.

	1	2	3	4
ASE	324.8	342.6	363.6	386.4

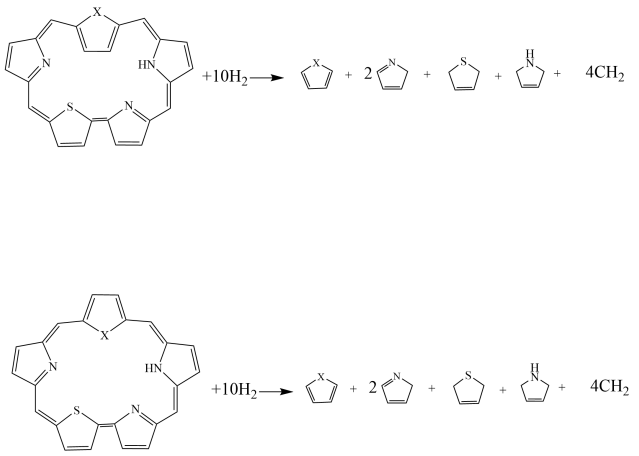

Scheme 2. The homodesmic schemes of **1**-**4.**

Table 3. NICS $(1)_{zz}$ values for **1-4** in the ground state.

NICS (ppm)	**1**	**2**	**3**	**4**
a thiophene / selenophene ring NICS $(1)_{zz}$	-19.38	-19.62	-22.28	-22.56
b pyrrole ring NICS $(1)_{zz}$	-1.32	-1.56	-1.54	-1.62
c pyrrole ring NICS $(1)_{zz}$	-1.67	-1.98	-1.37	-1.28
d thiophene ring NICS $(1)_{zz}$	-18.32	-18.64	-21.21	-21.83
e pyrrole ring NICS $(1)_{zz}$	-1.02	-1.36	-1.82	-1.25
f intramolecular critical point NICS $(1)_{zz}$	-17.42	-18.36	-17.18	-18.42
g intramolecular critical point NICS $(1)_{zz}$	-18.39	-19.20	-18.32	-19.14
h intramolecular critical point NICS $(1)_{zz}$	-17.26	-18.63	-18.71	-18.36
i intramolecular critical point NICS $(1)_{zz}$	-18.23	-17.83	-17.28	-19.31
j molecular ring center NICS $(1)_{zz}$	-16.76	-17.18	-18.01	-18.28

3.2 Aromaticity and electron delocalization

To further investigate the aromaticity of the designed molecules, we employed the nucleus-independent chemical shift (NICS) as a quantitative metric. Specifically, we focused on the representative NICS(1)zz values, which have been validated as reliable indicators of aromaticity in the S_0 state [35]. Typically, highly negative NICS(1)zz values indicate strong aromaticity, whereas positive values denote antiaromaticity. Furthermore, more negative NICS values correlate with increased stability. This approach, illustrated in Scheme 1, has been widely utilized for assessing the aromaticity and stability of porphyrins [36].

Table 3 presents the calculated NICS(1)zz values for molecules **1**–**4** in their ground states. Notably, all NICS(1)zz values at 1 Å above critical points *a*–*j* are negative, confirming the aromatic nature of these molecules. At critical point *a*, the NICS(1)zz values are -19.38, -19.62, -22.28, and -22.56 ppm for molecules **1**–**4**, respectively, indicating that normal thiophene and selenophene rings exhibit greater stability than their inverted counterparts. Furthermore, at critical point *d*, the thiophene moiety in molecules **3** and **4** displays higher aromaticity than in molecules 1 and 2. Similar trends are observed for NICS(1)zz values at 1 Å above critical points *b, c,* and *e*, as well as at intramolecular critical points *f, g, h,* and *i*. At the molecular center, the NICS(1) values in the ground state are -16.76, -17.18, -18.01, and -18.28 ppm for molecules **1**–**4**, respectively, demonstrating an increasing trend in aromaticity in the order of **1** < **2** < **3** < **4**. Additionally, molecules with conventional thiophene/selenophene moieties exhibit greater stability than those

with inverted structures. Notably, selenium-containing molecules (**3** and **4**) are more stable than their sulfur-containing counterparts (**1** and **2**), consistent with previous studies [37,38]. For comparison, the NICS(1) value of porphyrin is only -16.15 ppm [39], indicating that all designed molecules exhibit stronger aromaticity than porphyrin. Overall, these findings provide valuable insights into the aromaticity and stability of the designed molecules, highlighting their potential for applications in various fields.

Understanding the frontier molecular orbitals (FMOs) [40,41] is essential for evaluating the aromaticity and stability of molecules. The energy levels of the highest occupied molecular orbital (HOMO), lowest unoccupied molecular orbital (LUMO), and their energy gap (ΔH-L) serve as key indicators of molecular stability. Figure 2 presents the FMO diagrams and energy levels of HOMO, HOMO-1, LUMO, LUMO+1, and ΔH-L for molecules **1**–**4**. The HOMO, HOMO-1, LUMO, and LUMO+1 exhibit delocalization across the entire π-conjugated backbone. Specifically, the HOMO and HOMO-1 correspond to π-bonding orbitals, while the LUMO and LUMO+1 represent π*-antibonding orbitals. These molecules undergo π→π* transitions and conform to the four-orbital theory of porphyrins [42]. This orbital distribution facilitates intramolecular charge transfer, contributing to molecular stability. A larger HOMO-LUMO gap typically indicates lower susceptibility to optical excitation and greater stability. The calculated HOMO-LUMO gaps for molecules **1** (0.06 eV), **2** (0.08 eV), **3** (0.13 eV), and **4** (0.15 eV) are shown in Figure 2. Notably, molecules **3** and **4** exhibit larger gaps than molecules **1** and **2**, suggesting enhanced stability. Additionally, a positive correlation is observed between the absolute value of NICS(1)zz and the HOMO-LUMO energy gap, indicating that larger energy gaps correspond to more negative NICS(1)zz values. Overall, among the studied molecules, **2** is more stable than **1**, and **4** is more stable than **3**. Furthermore, replacing the pyrrole nitrogen atom with a Se heteroatom results in a more stable structure compared to S substitution.

Second-order perturbation energy is a key parameter in assessing the strength of stabilizing interactions between the lone pairs of S/Se heteroatoms in thiophene/selenophene and the π-antibonding C–C orbitals, as revealed by Natural Bond Orbital (NBO) analysis. For molecules **1**–**4**, the second-order perturbation energy values are 44, 42, 20, and 17 kcal/mol, respectively. These results suggest that the Se heteroatom in selenophene exhibits greater lone-pair delocalization than the S heteroatom in thiophene. Consequently, replacing the pyrrole nitrogen atom with a Se heteroatom leads to a more stable structure compared to S substitution.

3.3. Absorption and emission spectra

The TD-DFT method was employed to calculate the vertical electronic excitations, and the simulated electronic configurations are summarized in Table 4. The fitted Gaussian-type absorption curves are presented in Figure 3. It is well known that porphyrins exhibit distinct absorption features, primarily in the Soret (S) and Q bands [43]. As shown in Figure 3, all four designed molecules (**1**–**4**) display major absorption bands in the ultraviolet-visible region, closely resembling the absorption spectrum of porphyrins in terms of position. For molecules **1** and **2**, the dominant electronic transition corresponds to HOMO → LUMO+1, whereas for **3** and **4**, the major transition is HOMO → LUMO. Notably, the presence of a selenophene ring results in significantly red-shifted and intensified absorption compared to the thiophene-containing counterparts. Additionally, conventional thiophene/selenophene structures exhibit blue-shifted absorptions compared to their inverted configurations. Among the studied molecules, compound **4** exhibits the lowest-lying excitation at 657 nm, with a major HOMO → LUMO transition and a maximum oscillator strength of 1.208. The fitted Gaussian-type emission spectra are shown in Figure 4. TD-DFT, a well-established method for simulating molecular emission spectra, was used to calculate the emission energies, yielding values of 1. 54, 1.45, 1.85,

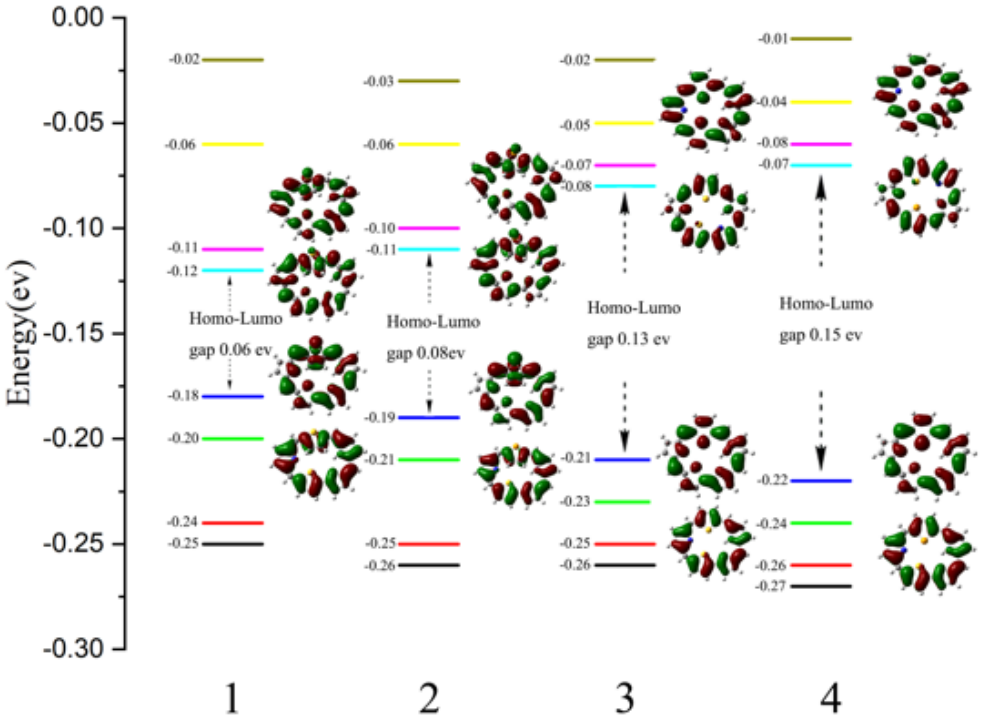

Figure 2. Molecular orbital distributions and diagrams of the frontier molecular orbitals (from HOMO-3 to LUMO+3) for **1**, **2**, **3** and **4.**

Table 4. Calculated absorption features of **1-4**.

Molecules	E/nm (eV)	Major contribution	Oscillator strength
1	756(1.64)	HOMO→LUMO+1 (51%) HOMO-1→LUMO+1(44%)	1.016
2	793(1.56)	HOMO→LUMO+1 (45%) HOMO-1→LUMO (39%)	1.049
3	624 (1.99)	HOMO→LUMO (52%) HOMO-1→LUMO (47%)	1.156
4	657 (1.89)	HOMO→LUMO (53%) HOMO-1→LUMO+1 (46%)	1.208

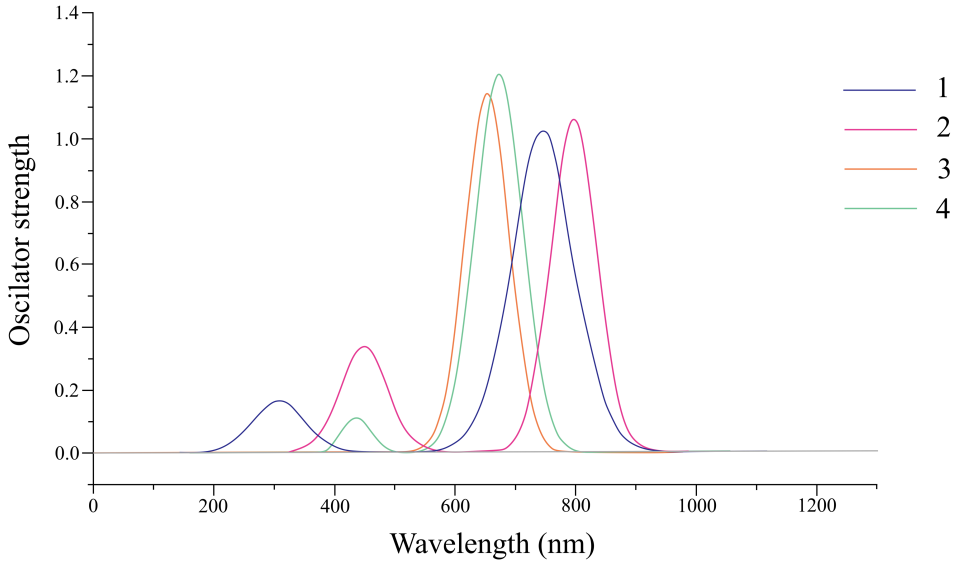

Figure 3. The fitted Gaussian type absorption spectra based on the TD-DFT/CAM-B3LYP/6-311G (d, p) calculation for molecules **1-4.**

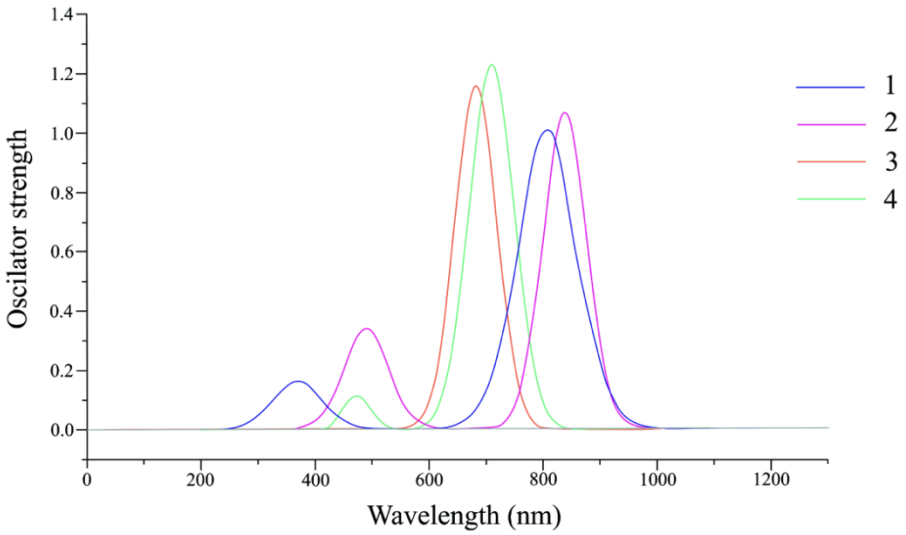

Figure 4. The fitted Gaussian type emission spectra for molecules **1-4.**

and 1.75 eV for molecules 1, 2, 3, and 4, respectively. Furthermore, the calculated Stokes shifts, defined as the energy difference between the lowest-lying absorption and emission spectra, range from 0.1 to 0.14 eV.

4. Conclusions

In summary, we conducted a comprehensive theoretical investigation into the aromaticity, stability, and photophysical properties of molecules **1**–**4**, incorporating thiophene and selenophene units into expanded porphyrins. Using DFT and TD-DFT calculations, we established a direct correlation between molecular stability and aromaticity, as assessed by ΔH-L values and NICS(1)zz values. Notably, all designed molecules exhibit stronger aromaticity than porphyrin. Our findings indicate that molecules with conventional thiophene or selenophene rings exhibit superior stability compared to their inverted counterparts, owing to their enhanced coplanarity. As a result, molecules **3** and **4** are more likely to form π–π stacking interactions. Additionally, substitution of the pyrrole nitrogen with a selenium (Se) heteroatom increases the HOMO–LUMO energy gap, reducing susceptibility to optical excitation and enhancing molecular stability compared to sulfur (S) heteroatoms. The absorption spectra of all four molecules align with porphyrins, featuring prominent Soret and Q bands. These absorption characteristics primarily arise from HOMO → LUMO+1 or HOMO → LUMO transitions, facilitating intramolecular charge transfer. Among the designed molecules, compound **4** stands out due to its larger HOMO–LUMO energy gap, more planar structure, and stronger aromaticity. Overall, these theoretical insights provide a valuable foundation for the future design and development of novel expanded porphyrin materials with enhanced stability and optoelectronic properties.

Acknowledgments

We gratefully acknowledge HZWTECH for providing computation facilities.

References

[1] Tang Z., Jiang Z., Chen H. J., Su P. F., Wu W. Energy decomposition analysis based on broken symmetry unrestricted density functional theory. *J. Chem. Phys.*, **151** (2019), 244106.

[2] Wang S. Y., Yuan X. X., Pang L. J., Song P. L., Jia R. F., Song X. Q. Establishment of an assistive diagnostic model for schizophrenia with oxidative stress biomarkers. *Frontiers in Pharmacology*, **14** (2023).

[3] Lomova T. N. The p-metal porphyrins: from specificity of properties to application in medicine, catalysis, and optoelectronics. *Macroheterocycles*, **14** (2021), 299–311.

[4] Moura N. M. M., Faustino M. A. F., Neves M. G. P. M. S. Tetrapyrrolic macrocycles: synthesis, functionalization and applications 2018. *Molecules*, **25** (2020), 433.

[5] Huang H. H., Chen K., Li T. T. Porphyrin and phthalocyanine based covalent organic frameworks for electrocatalysis. *Coord. Chem. Rev.*, **464** (2022), 214563.

[6] Menendez M. I., Montenegro-Pohlhammer N., Pino-Rios R., Urzua-Leiva R., Morales-Lovera S., Borges-Martínez M., Granados-Tavera K., Lopez R., Cardenas-Jiron G. Near-infrared absorption of fused core-modified expanded porphyrins for dye-sensitized solar cells. *J. Chem. Phys.*, **158** (2023).

[7] Casademont-Reig I., Woller T., Garcia V., Contreras-Garcia J., Tiznado W., Torrent-Sucarrat M., Matito E., Alonso M. Quest for the most aromatic pathway in charged expanded porphyrins. *Chemistry* (Weinheim an der Bergstrasse, Germany), **29** (2023), e202202264.

[8] Sen S., Ishiwari F., Kaur R., Ishida M., Ray D., Kikuchi K., Mori T., Bähring S., Lynch V. M., Saeki A., Guldi D. M., Sessler J. L., Jana A. Supramolecular recognition within a nanosized "buckytrap" that exhibits substantial photoconductivity. *J. Am. Chem. Soc.*, **145** (2023).

[9] Figueira F., Paz F. A. A., Tome J. P. C. Meso pyridin-4-ylsulfanyl substituted doubly N-confused pentafluorophenyl[26]hexaphyrin. *J. Porphyrins Phthalocyanines*, **27** (2023), 1042–1048.

[10] Tanaka T., Osuka A. Chemistry of meso-aryl-substituted expanded porphyrins: aromaticity and molecular twist. *Chem. Rev.*, **117** (2017), 2584–2640.

[11] Alka A., Shetti V. S., Ravikanth M. Coordination chemistry of expanded porphyrins. *Coord. Chem. Rev.*, **401** (2019), 213063.

[12] Zheng X., Zhong J., Dong M. Y., Wen Y., Chen A. Z. Synthesis of porphyrin-based 2D ytterbium metal organic frameworks for efficient photodynamic therapy. *RSC Adv.*, **12** (2022), 34318–34324.

[13] Li Q. Z., Ishida M., Wang Y. Y., Li C. J., Baryshnikov G., Zhu B., Sha F., Wu X. Y., Ågren H., Furuta H., Xie Y. S. Antiaromatic sapphyrin isomer: transformation into contracted porphyrinoids with variable aromaticity. *Angew. Chem. Int. Ed.*, **62** (2023), e2022121.

[14] Sahoo S. S., Sahoo S., Panda P. K. Monothia [22]pentaphyrin(2.0.1.1.0): a core-modified isomer of sapphyrin. *Dalton Trans.*, **51** (2022), 6526–6532.

[15] Richter D. T., Lash T. D. Synthesis of sapphyrins, heterosapphyrins, and carbasapphyrins by a "4 + 1" approach. *J. Org. Chem.*, **69** (2004), 8842–8850.

[16] Isar P., Ravikanth M. Dibenzoylbenzodipyrroles: key precursors for the synthesis of fused meso-aryl sapphyrins. *J. Org. Chem.*, **85** (2020), 7287–7296.

[17] Jeong S. D., Sessler J. L., Lynch V., Lee C. H. Dithiabenzisapphyrin: a core-modified sapphyrin bearing exocyclic double bonds at the meso-positions. *J. Am. Chem. Soc.*, **130** (2008), 390–391.

[18] Rao Y. T., Zhou W. J., Xu L., Zhou M. B., Yin B. S., Tanaka T., Osuka A., Song J. X. Singly and doubly neo-confused smaragdyrins. *J. Am. Chem. Soc.*, **141** (2019), 18836–18844.

[19] Nipate A. B., Rao M. R. Solid-state red-emissive (cyano)vinylene heteroaromatics via Pd-catalysed C–H homocoupling. *Org. Biomol. Chem.*, **21** (2023).

[20] Spergen A., Kalaiselvan A., Gokulnath S. Near-IR electrochromic dihydroindolo(2,3-a)carbazole-based macrocycles and their [b]-annulated BODIPY complexes. *Adv. Optical Mater.*, **11** (2023), 2300778.

[21] Robbins E., Deska R., Slusarek K., Dudek M., Samoc M., Latos-Grazynski L., Szyszko B., Matczyszyn K. Two-photon absorption of 28-hetero-2,7-naphthiporphyrins: expanded carbaporphyrinoid macrocycles. *RSC Adv.*, **12** (2022), 19554–19560.

[22] Sengupta R., Ravikanth M., Chandrashekar T. K. Inverted and fused expanded heteroporphyrins. *Chem. Soc. Rev.*, **50** (2021), 13268–13320.

[23] Rawat N., Thorat K. G., Kumar S., Ravikanth M. Synthesis of expanded hetero 2,6-pyrihexaphyrins. *Eur. J. Org. Chem.*, **2020** (6) (2020), 736–743.

[24] Sahoo S., Jana M., Rath H. Tailor-made aromatic porphyrinoids with NIR absorption. *Chem. Commun.*, **58** (2022), 1834–1859.

[25] Ji M., Zhen J. F., Zhang Q., Chen Y. Photolysis of n-butyl nitrite and isoamyl nitrite at 355 nm: a time-resolved Fourier transform infrared emission spectroscopy and ab initio study. *J. Chem. Phys.*, **130** (2009), 174314.

[26] Suzuki T., Yokomizo Y. Energy bands of atomic monolayers of various materials: possibility of energy gap engineering. *Physica E*, **42** (2010), 2820–2825.

[27] Li Z., Xiao Y., Liu W. On the spin separation of algebraic two-component relativistic Hamiltonians. *J. Chem. Phys.*, **137** (2012), 154114.

[28] Li Z., Suo B., Zhang Y., Xiao Y., Liu W. Combining spin-adapted open-shell TD-DFT with spin–orbit coupling. *Mol. Phys.*, **24** (2013), 3741–3755.

[29] Yang Y. F., Cheng G. J., Zhu J., Zhang X., Inoue S., Wu Y. D. Silicon-containing formal 4π-electron four-membered ring systems: antiaromatic, aromatic, or nonaromatic? *Chem. Eur. J.*, **18** (2012), 7516–7524.

[30] Frisch M., Trucks G. W., Schlegel H. B., Scuseria G. E., Robb M. A., Cheeseman J. R., Scalmani G., Barone V., Petersson G. A., Nakatsuji H., Li X., Caricato M., Marenich A. V., Bloino J., Janesko B. G., Gomperts R., Mennucci B., Hratchian H. P., Ortiz J. V., Izmaylov A. F. *Gaussian16 Revision A.03*, Gaussian Inc., Wallingford, CT, 2016.

[31] Bader R. F. W., Popelier P. L. A., Keith T. A. Theoretical definition of a functional group and the molecular orbital paradigm. *Angew. Chem. Int. Ed. Engl.*, **33** (1994), 620–631.

[32] Biegler-König F., Schönbohm J., Bayles D. AIM2000 – a program to analyze and visualize atoms in molecules. *J. Comput. Chem.*, **22** (2001), 545–559.

[33] Reed A. E., Curtiss L. A., Weinhold F. Intermolecular interactions from a Natural Bond Orbital, donor-acceptor viewpoint. *Chem. Rev.*, **88** (1988), 899–926.

[34] Cyranski M. K., Schleyer P. v. R., Krygowski T. M., Jiao H. J., Hohlneicher G. Facts and artifacts about aromatic stability estimation. *Tetrahedron*, **59** (2003), 1657–1665.

[35] Sun H. C., An K., Zhu J. Triplet state aromaticity: NICS criterion, hyperconjugation, and charge effects. *Chem. Asian J.*, **11** (2016), 234–240.

[36] Jeon K. O., Jun J. H., Yu J. S., Lee C. K. Mass spectroscopical properties of benzoyl derivatives of five-membered monoheterocycles and determination of aromaticity indices. *Bull. Korean Chem. Soc.*, **25** (2004), 1840–1844.

[37] Yoon M. C., Misra R., Yoon Z. S., Kim K. S., Lim J. M., Chandrashekar T. K., Kim D. Photophysical properties of core-modified expanded porphyrins: nature of aromaticity and enhancement of ring planarity. *J. Phys. Chem. B*, **112** (2008), 6900–6905.

[38] Bhattacharyya P. K. A DFT study on reactivity, aromaticity and absorption spectra of perylo[1,12-b,c,d]thiophene tetraester doped with B, N, O, Se and BN. *Comput. Theor. Chem.*, **1082** (2016), 29–40.

[39] Kiran B., Nguyen M. T. Density functional studies on n-fused porphyrin, electronic, magnetic and metal binding properties. *J. Organomet. Chem.*, **643** (2002), 265–271.